Atomic distribution and local structure in charge-ordered $La_{1/3}Ca_{2/3}MnO_3$

F. L. Tang and X. Zhang*
Laboratory of Advanced Materials, Department of Materials Science and Engineering, Tsinghua University, Beijing 100084, People's Republic of China

(Received 3 November 2005; revised manuscript received 5 January 2006; published 3 April 2006)

Atomic simulation has been performed to investigate atomic distribution and local structure in $La_{1/3}Ca_{2/3}MnO_3$. It is found that La/Ca ordering along with Mn^{3+} and Mn^{4+} stripes is more energetically favorable than La/Ca disordering at low temperature (0–50 K). Apart from the Wigner-stripe and bistripe models, the simulation reveals another possible and energetically stable charge-ordered model: a layer-stripe model with La^{3+} and Mn^{3+} ions forming a $LaMnO_3$-like local structure, whereas Ca^{2+} and Mn^{4+} form a $CaMnO_3$-like local structure. It is also found that in these three stripe models, especially in the layer-stripe model, the local structure is very different from its average structure. It is expected that such cation distribution and local structure may be a compositional and structural representation of phase separation in doped manganites.

DOI: 10.1103/PhysRevB.73.144401 PACS number(s): 75.47.Gk, 74.62.Dh

I. INTRODUCTION

The discovery of colossal magnetoresistance (CMR) in rare-earth manganites, $La_{1-x}A_xMnO_3$ (A=Ca, Sr, and Ba) with perovskite structure, has attracted much attention for their rich display of interesting basic-physics problems and possible applications.[1–3] One of the most important aspects of the physics in doped manganites was the finding of charge-ordered phases, which may affect transport and magnetic properties of these compounds.[4–8]

Some earlier studies focused on the real-space images of charge ordering and proposed some crystal models to illustrate these images. Chen *et al.*[4] studied charge-ordered stripes in $La_{0.33}Ca_{0.67}MnO_3$ by use of electron diffraction (ED) and transmission electron microscopy (TEM). They illustrated these stripes as the Wigner-crystal model with a periodic spacing of $3a \approx 16.5$ Å. They believed that the stripes extended along both the a and b directions (in *pbnm* symmetry). With the same TEM technique, Mori *et al.* illustrated the charge-ordered Mn^{3+} and Mn^{4+} stripes in $La_{0.33}Ca_{0.67}MnO_3$ as the bistripe model.[5] Radaelli *et al.*[7] used high-resolution synchrotron x-ray and neutron powder diffraction techniques to study the crystallographic (charge-ordered) and magnetic structures of $La_{0.33}Ca_{0.67}MnO_3$. They believed that the charge-ordered arrangement of Mn^{3+} and Mn^{4+} ions was very likely to be the Wigner-crystal model. Using the same techniques as Radaelli *et al.*, Fernández-Díaz *et al.*[6] also supported the Wigner-crystal model of the charge-ordered stripes, but believed that the bistripe model was not entirely impossible. Fernández-Díaz *et al.*[6] proposed that charge ordering was along both the a and c directions, whereas Radaelli *et al.*[7] proposed that charge ordering was only along the a direction. Wang *et al.*[8] used quantitative ED and high-resolution imaging to distinguish the Wigner-stripe model from the bistripe model in $La_{0.33}Ca_{0.67}MnO_3$. They found that the possibility of charge ordering along the c direction was small.

Besides Mn ions distribution, the distribution of the doped divalent ions, such Ca, Sr, or Ba ions were also studied. Some researchers believed that Ca and Sr were randomly distributed.[6–10] However, Mori *et al.*[5] found some sort of "clustering" effect in $La_{1-x}Ca_xMnO_3$, whereas Shibata *et al.*[11] indicated a tendency for Sr clustering in $La_{1-x}Sr_xMnO_3$. It was also reported that in $La_{0.5}Ba_{0.5}MnO_3$ doped Ba cations distributed orderly: the MnO_2 square sublattice sandwiched by LaO and BaO rock-salt layer, with different lattice sizes.[12–15] A calculation[16] of $La_{0.5}Sr_{0.5}MnO_3$ showed that the Sr-O plane and La-O plane emerged alternately. Films of $La_{2/3}Ca_{1/3}MnO_3$ were prepared via atomic layer-by-layer epitaxy as La-site ordered superlattice layers.[17] La-ordered and La-disordered structures could be prepared with different preparation methods.[12,13,15,17]

Although plenty of experimental results were given to understand the structure of charge-ordered phases in doped manganites, there are still some controversies and discrepancies: (i) How the doped ions (Ca, Sr, or Ba) distribute in the charge-ordered stripes? (ii) Apart from the Wigner-stripe and bistripe model, is there any other possible charge-ordered model? (iii) Can the stripes be along both the a and c directions? (We assigned the long, medial, and short lattice parameters as b, a, and c, respectively.) (iv) Is the local structure of the charge-ordered stripe the same as the average structure?

For investigating the above four questions, we used an atomic simulation technique to study atomic distribution and local structure in $La_{1/3}Ca_{2/3}MnO_3$. In Sec. II, we describe the atomic simulation method and test the potential parameters used in this work by pressure and temperature effect on manganites. In Sec. III, we present the calculated lattice energy and lattice parameters for different atomic distributions and compare the calculated results with the experimental results. The local structures of charge-ordered $La_{1/3}Ca_{2/3}MnO_3$ are also presented by comparing the calculated Mn-O and La/Ca-Mn bond lengths with some experimental data. Section IV summarizes our conclusions.

II. COMPUTATIONAL METHODS

The crystal structure of a material at a given temperature and pressure can be predicted by minimizing its free energy. Our approach is to adjust the cell volume and atomic positions until the net pressure or stress is zero. The pressure P is simply the derivative of the free energy F with respect to volume V. Thus for a cubic material:

$$P = dF/dV. \quad (1)$$

Calculating the free energy at a given volume and then recalculating it after making a small adjustment to the cell volume dV determines the pressure.

During the iterative procedure, a constant volume energy minimization is performed. Hence, each time the cell volume is modified; all atomic positions are adjusted so that they remain at a potential energy minimum. Thus by minimizing to constant pressure and including the vibrational component of the free energy, the crystal structure at a given temperature and pressure can be predicted. This technique has been used for simulation of many kinds of materials.[18–28] Details of this technique are available in Ref. 29.

Our simulation is based on the widely used successful shell model[30] generalization of the Born model of a solid. With this model, the lattice energy E can be expressed as

$$E = \frac{1}{2}\sum_{i,j}\left[\frac{q_i q_j}{r_{ij}} + V(r_{ij})\right], \quad (2)$$

where the first item is Coulombic energy introduced by long-range interactions of effective charges, and the second item is the short-range interaction. Short-range interaction is represented by a Buckingham potential

$$V(r) = A\exp(-r/\rho) - Cr^{-6}, \quad (3)$$

where A, ρ, and C are fitting parameters. In order to describe the polarization of an individual ion and its dependence on local atomic environment, it is treated by the core-shell model.[30] The interaction between the core and shell of any ion is treated as harmonic with a spring constant k and is represented by

$$E_v(d_i) = \frac{1}{2}kd_i^2, \quad (4)$$

where d_i is the relative displacement of core and shell of ion i. The polarization of a massless shell with Y charge and a core with X charge ($X+Y$ is the charge of the ion) can be calculated as

$$\alpha = \frac{Y^2}{k}, \quad (5)$$

where Y is the charge of the shell, relating to dielectric constant, and k is the force constant between core and shell, relating to the phonon frequency. Both parameter Y and k are fitting parameters.

The potential parameters for $LaMnO_3$ and $CaMnO_3$ are obtained at 0 K by an empirical method, known as the "relaxed" fitting approach, the structure is relaxed to zero strain for every evaluation of the sum of squares and the difference between the observed and calculated structural parameters is used in place of the derivatives. In each step in the fitting, the minimization is started from the experimental structure to avoid the possibility that the fit becomes trapped in an undesirable local minimum in either potential of geometry space.

TABLE I. Potential parameters for $LaMnO_3$: short-range interaction and shell model parameters.

	Short-range interaction		
	A (eV)	ρ (Å)	C (eV Å^6)
$O(1)^{2-}$-$O(1)^{2-}$	22764.3000	0.1490	43.0
$O(2)^{2-}$-$O(2)^{2-}$	22764.3000	0.1490	43.0
$O(1)^{2-}$-$O(2)^{2-}$	22764.3000	0.1490	43.0
La^{3+}-$O(1)^{2-}$	2800.0828	0.3274	0.0
La^{3+}-$O(2)^{2-}$	23533.3281	0.2447	0.0
Mn^{3+}-$O(1)^{2-}$	8474.5750	0.2392	0.0
Mn^{3+}-$O(2)^{2-}$	344.0376	0.4431	0.0
	Shell-model parameters		
Species	Y (e)	K (eV Å^{-2})	
La^{3+}	−0.250	145.0	
Mn^{3+}	3.000	95.0	
$O(1)^{2-}$	−2.389	42.0	
$O(2)^{2-}$	−2.389	42.0	

It should be stressed that the reliability of the simulations depends on the validity of the potential model used in the calculation, and the latter is assessed primarily by its ability to reproduce experimental crystal properties. The available potential parameters of $LaMnO_3$ that we used are given in Table I.[28] We use different potential parameters for bonds of Mn^{3+}-O1, Mn^{3+}-O2, La-O1, and La-O2 so that the potentials can describe the directions of orbits of Mn^{3+} d electrons and Jahn-Teller effects. This potential can reproduce the experimental crystal structure of $LaMnO_3$ with the differences in lattice parameters between the calculated and experimental data less than 1.0%. The differences in bond lengths between the calculated and experimental data are less than 1.5% except for the bond lengths La-O1(2) and La-O1(4) (we denoted the O^{2-} ions along b axis as O1, the O^{2-} ions on the a-c plane as O2 of the MnO_6 octahedra) which have the largest errors of 3.04% and 3.7%, respectively.[28] In order to further examine the validity of our potential model, we calculated the pressure effect on lattice parameters of $LaMnO_3$ up to pressure of 3.4 GPa. The calculated results of pressure effect on the cell volume and lattice parameters of $LaMnO_3$ are shown in Figs. 1(a) and 1(b). It is found that as the pressure increases the cell volume decreases, the parameter a decreases significantly, c decreases just a little, and b almost remains unchanged. The decrease of cell volume mainly arises from the decrease of lattice parameter a. The calculated compressibility of V, a, b, and c are 10.0×10^{-3} GPa^{-1}, 9.0×10^{-3} GPa^{-1}, -0.12×10^{-3} GPa^{-1}, and 1.1×10^{-3} GPa^{-1}, respectively. The corresponding experimental values are 8.1×10^{-3} GPa^{-1}, 6.1×10^{-3} GPa^{-1}, 0.96×10^{-3} GPa^{-1}, and 1.3×10^{-3} GPa^{-1}, respectively, when $P<3.5$ GPa.[31] The calculated results of the compressibility are in agreement with the experimental results except for the compressibility of the lattice parameter b, indicating that the potentials we used can represent the crystal structure of $LaMnO_3$.

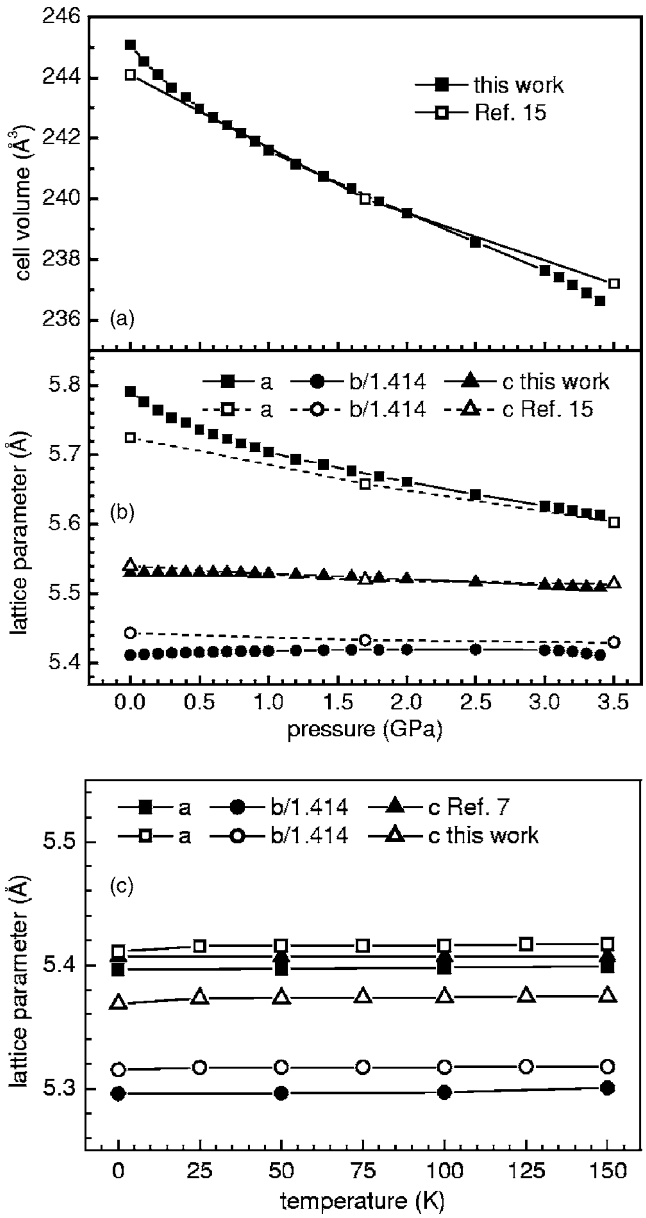

FIG. 1. Comparison of calculated and experimental results of pressure effect on volume (a) and lattice parameters (b) of $LaMnO_3$. Comparison of calculated and experimental results of temperature effect on lattice parameters of $La_{0.333}Ca_{0.667}MnO_3$ (c).

The potential parameters of $CaMnO_3$ that we developed are given in Table II.[28] For $CaMnO_3$, the differences in lattice parameters and the differences in bond length between the calculated and experimental data are less than 0.3% and 1.2%, respectively. This shows that the potentials we used can represent the crystal structure of $CaMnO_3$.

We have also investigated the vibrational contributions of Ca-doped $LaMnO_3$ at some low temperatures to further test our potentials shown in Tables I and II. For studying the temperature effect on lattice and charge ordering, one charge-ordered stripe configuration is heated from 0 K to 150 K. It is found that the lattice parameters [Fig. 1(c)] are almost unchanged when the temperature changes. This result is consistent with the experimental results,[6,7] indicating that the potentials we used are stable and suitable at low temperature (<150 K). The size effect in simulation is also considered. For different sizes of the supercell of $LaMnO_3$ containing four to nine unit cells, the variation in lattice energy is less than 0.001 eV and the variation in lattice parameters is less than 0.0001 Å. Therefore, the size effect can be neglected in our simulation.

TABLE II. Potential parameters for $CaMnO_3$: short-range interaction and shell model parameters.

	Short-range interaction		
	A (eV)	ρ (Å)	C (eV Å^6)
$O(1)^{2-}$-$O(1)^{2-}$	22764.3000	0.1490	43.0
$O(2)^{2-}$-$O(2)^{2-}$	22764.3000	0.1490	43.0
$O(1)^{2-}$-$O(2)^{2-}$	22764.3000	0.1490	43.0
Ca^{2+}-$O(1)^{2-}$	32525.0215	0.2148	0.0
Ca^{2+}-$O(2)^{2-}$	26312.4043	0.2197	0.0
Mn^{4+}-$O(1)^{2-}$	16526.0604	0.2218	0.0
Mn^{4+}-$O(2)^{2-}$	16741.0424	0.2217	0.0
	Shell-model parameters		
Species	Y (e)	K (eV Å^{-2})	
Ca^{2+}	2.000	110.2	
Mn^{4+}	4.000	95.0	
$O(1)^{2-}$	–2.389	42.0	
$O(2)^{2-}$	–2.389	42.0	

In this work, the initial structure we started for studying the $La_{1/3}Ca_{2/3}MnO_3$ is the crystallographic unit cell of $LaMnO_3$, which has four La^{3+} ions, four Mn^{3+} ions, four O1 ions, and eight O2 ions. To meet the demand of the ions number proportion in $La_{1/3}Ca_{2/3}MnO_3$ and make the calculations most efficient, the unit cell of $LaMnO_3$ is extended to three times along both the a- and c-axis directions. There are 36 La^{3+}, 36 Mn^{3+}, and 108 O^{2-} ions in the extended supercell. For simulating the structure of $La_{1/3}Ca_{2/3}MnO_3$, 24 La^{2+} and 24 Mn^{3+} ions are substituted by Ca^{2+} and Mn^{4+} ions, respectively.

III. RESULTS AND DISCUSSION

A. Atomic distribution

Just as was mentioned in the Introduction, two types of charge-ordered stripes: the Wigner model and the bistripe model with a periodic spacing of $a_{CO}=3a\approx 16.5$ Å,[4–8] schematically illustrated in Figs. 2(a) and 2(b), had been investigated in detail. If one extends the charge-ordered unit cell of these two models along the c_{CO}-axis direction periodically, Mn^{3+} and Mn^{4+} ions will form charge-ordered stripes: the Wigner model emerges as 344344 stripes (3 denotes a Mn^{3+} stripe and 4 denotes a Mn^{4+} stripe along c_{CO} direction), and the bistripe as 434443. However, our simulation revealed another arrangement of Mn^{3+} and Mn^{4+}: 334444 [Fig. 1(c)], hypothetically called a layer stripe for convenience in this paper. Apart from these three kinds of stripes, no other stripe

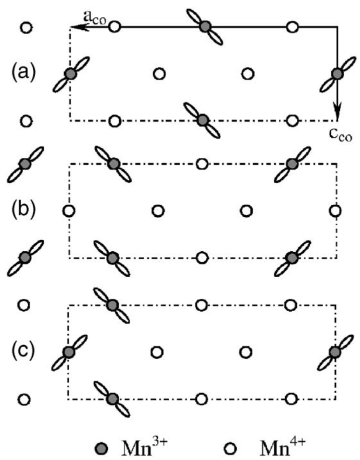

FIG. 2. Wigner-stripe model (a), bistripe model (b), and a possible layer-stripe model (c) of charge ordering in $La_{1/3}Ca_{2/3}MnO_3$.

model with a periodic spacing of $3a$ was found in our simulation.

In order to investigate the arrangement of the atoms in $La_{1/3}Ca_{2/3}MnO_3$, firstly, we simulated 250 configurations in which both La^{3+}/Ca^{2+} and Mn^{3+}/Mn^{4+} ions were all randomly distributed. It is found that for some random configurations the simulation processes could not converge. Most calculated lattice parameters of the random configurations deviated from experimental data very much, and the calculation result of one configuration was always very much different from that of the others. The average results of 10 configurations with the least deviations from the experimental data are listed in Table III(a). Secondly, in order to investigate the effect of La/Ca distribution, Mn-ordered but La/Ca-disordered configurations were simulated (200 configurations for every kind of stripe, most of them converged). The average lattice energy and lattice parameters of the converged configurations are listed in Table III(b)–III(d), and the average results of all of them are listed in Table III(e). Finally, the bistripe, Wigner stripe, and layer stripe, along the *a* and *c* directions were simulated. All of them converged. In these stripes, La^{3+} ions and Ca^{2+} ions were also charge-ordered along with Mn^{3+} and Mn^{4+} ions, respectively. For these three models, the average lattice energy and lattice parameters of the ordered configurations along the two directions are listed in Table III(f)–III(h). The average results of all of them are listed in Table III(i).

From Table III, it is found that both La-site and Mn-site disordered configurations have the highest lattice energy

TABLE III. The average lattice energy and lattice parameters of the simulated configurations and some experimental lattice parameters of $La_{1/3}Ca_{2/3}MnO_3$.

	E (eV)	V (Å^3)	a (Å)	b (Å)	c (Å)
Random[a]	−634.07	221.87	5.4275	7.5625	5.4055
Bistripe[b]	−635.91	223.14	5.4615	7.4919	5.4535
Wigner-stripe[c]	−635.98	222.78	5.4653	7.5004	5.4348
Layer-stripe[d]	−635.92	222.59	5.4412	7.5567	5.4135
Average[e]	−635.94	222.84	5.4560	7.5164	5.4339
Bistripe[f]	−636.48	221.12	5.4218	7.5326	5.4143
Wigner-stripe[g]	−636.51	220.40	5.4241	7.5216	5.4023
Layer-stripe[h]	−636.65	218.53	5.3986	7.5230	5.3808
Average[i]	−636.55	219.86	5.4124	7.5262	5.3973
Experiment[j]	/	218.85	5.4067	7.5032	5.3948
Experiment[k]	/	218.84	5.3962	7.4988	5.4081
Experiment[l]	/	219.38	5.3812	7.5687	5.3864
Experiment[m]	/	218.80	5.3805	7.5639	5.3763
Experiment[n]	/	219.18	5.3679	7.6168	5.3607

[a]Average results of 10 selected random configurations, in which La/Ca and Mn ions are all disordered.
[b]Average results of La/Ca disordered configurations, in which Mn^{3+}/Mn^{4+} are ordered in bistripes.
[c]Average results of La/Ca disordered configurations, in which Mn^{3+}/Mn^{4+} are ordered in Wigner stripes.
[d]Average results of La/Ca disordered configurations, in which Mn^{3+}/Mn^{4+} are ordered in layer stripes.
[e]Average results of b, c and d.
[f]Average results of 2 bistripe configurations: one along a direction, the other along c direction.
[g]Average results of 2 Wigner-stripe configurations: one along a direction, the other along c direction.
[h]Average results of 2 layer-stripe configurations: one along a direction, the other along c direction.
[i]Average results of f, g and h.
[j]Ref. 6.
[k]Ref. 7.
[l]Ref. 8.
[m]Ref. 32. Lattice parameters are obtained by linear interpolating.
[n]Ref. 33.

(−634.07 eV per cell) though they have similar lattice parameters compared with experimental results [Table III(j)–III(n)[6–8,32,33]]. The La-site disordered but Mn-ordered configurations have somewhat lower lattice energy (−635.91 to −635.98 eV). The lattice parameters of Mn-ordered but La/Ca-disordered configurations deviate from the experimental data. The average results of the ordered configurations have the lowest lattice energy (−636.55 eV), 2.48 eV lower than that of the disordered configurations and 0.61 eV lower than that of the La-site disordered configurations. And the structure of the ordered configurations deviates from experimental structure very little. This means that charge-ordering stripes are the most energetically stable and structurally preferable configurations. Our simulations show that La/Ca ions are more energetically favorable to be orderly distributed with Mn-ordering at 0 K, rather than randomly distributed.

The experimental results showed that La-site disorder[6–10] and La-site order[12–17] manganites were obtained with different preparation conditions at high temperature. References 12–15 reported Ba-ordered and Ba-disordered $La_{0.5}Ba_{0.5}MnO_3$. Reference 11 found Sr clusters in lightly doped $La_{1-x}Sr_xMnO_3$. The local structural disorder in the vicinity of the clustered Sr ions is also significantly smaller than in the vicinity of clustered La ions, presumably attributable to a higher average Mn^{3+} concentration near the La regions. A calculation[16] of $La_{0.5}Sr_{0.5}MnO_3$ adopted a supercell in which Mn^{3+} was in the vicinity of La^{3+}, whereas Mn^{4+} was in the vicinity of Sr^{2+}. This calculation showed that Sr-O plane and La-O plane emerged alternately. The La/Sr distribution is very similar to La/Ca distribution of our layer stripe $La_{1/3}Ca_{2/3}MnO_3$. Films of $La_{2/3}Ca_{1/3}MnO_3$ were prepared via atomic layer-by-layer epitaxy both as standard solid-solution alloys and La-site ordered superlattice layers. The La-site ordered films consisted of two pseudocubic unit-cell layers of $LaMnO_3$ and one pseudocubic unit-cell $CaMnO_3$.[17] We also performed La-site order and disorder simulations on $La_{2/3}Ca_{1/3}MnO_3$. The average lattice energy of La-site disordered configurations is larger than that of the La-site ordered ones by about 0.2 eV (the average lattice energy is about −596 eV). Our simulated results of $La_{2/3}Ca_{1/3}MnO_3$ also show that La-site ordered configurations are more energetically favorable to La-site disordered configurations at 0 K. Like the layer stripe of $La_{1/3}Ca_{2/3}MnO_3$, the layer stripe of $La_{2/3}Ca_{1/3}MnO_3$ can be divided as two parts: the $LaMnO_3$-like layer that contains La^{3+} and Mn^{3+} ions, and the $CaMnO_3$-like layer that contains Ca^{2+} and Mn^{4+} ions. The width of the first part is about two times of the width of the second part. Our simulated layer structure of $La_{2/3}Ca_{1/3}MnO_3$ is similar to the experimental layer structure of $La_{2/3}Ca_{1/3}MnO_3$ reported by Ref. 17.

We also investigate the temperature effect on lattice energy of La-site ordered and disordered $La_{1/3}Ca_{2/3}MnO_3$ using our atomic simulation technique. The calculation cannot converge when the temperature is larger than 150 K in the case of La-site order or larger than 50 K in the case of La-site disorder. The lattice energy will only increase by less than 0.004 eV (for La-site order, from 0 K to 150 K) or less than 0.002 eV (for La-site disorder, from 0 K to 50 K). This indicates that temperature has very little effect on La-site ordering at low temperatures. Although our calculation results at 0 K show that La-site ordered $La_{1/3}Ca_{2/3}MnO_3$ is more stable than the La-site disordered one, we do not exclude the possibility of the La-site disorder at higher temperatures.

Among the charge-ordered stripes, the results of the Wigner stripes are almost the same as that of the bistripes. Their average cell volumes (220.40 Å^3 for the former and 221.12 Å^3 for the latter) are somewhat larger than the experimental data (they varied from 218.80 to 219.38 Å^3). The average cell volume of the layer stripes (218.53 Å^3) is closer to the experimental data than that of the other two stripes, indicating that the layer stripe is the most structurally reasonable atomic distribution. The layer-stripe model has also the least lattice energy (−636.65 eV) compared with the Wigner-stripe model (−636.51 eV) and the bistripe model (−636.48 eV), indicating that the layer-stripe model is the most energetically preferable configuration. Hence, we propose that the layer-stripe model may be another possible charge-ordered model besides the Winger- and bistripe models. In the layer-stripe model, the Mn^{3+} ions attempt to approach as close as possible so that this stripe model has the least lattice energy. Also, in the layer-stripe model, the charges around every Mn^{3+} or Mn^{4+} stripe can counteract themselves and this may result in the reduction of Coulombic energy.

In addition, one must notice that the difference in lattice energies among the three different ordered stripes is smaller than 0.17 eV. It is possible that all the Wigner-stripe, the bistripe, and the layer-stripe models can exist in doped manganites. We believe that these three stripes could exist in different $La_{0.33}Ca_{0.67}MnO_3$ produced with different forming conditions, even exist in the same $La_{0.33}Ca_{0.67}MnO_3$ with different local conditions (strains, crystal defects, grain boundaries, and so on). The coexistence of two nonferromagnetic phases has been observed recently in $La_{1-x}Ca_xMnO_3$ ($x=0.67$ and 0.71) at 90 K: a modulated charge-ordered phase and a modulation-free region composed of the monoclinic needle twin. And a tweed microstructure was observed in the interface region between these two phases.[34] The coexistence of lamellar charge-ordered domains with a sheet-like morphology and charge-disordered domains was also reported.[35] These experimental results indicate that the structure of manganite materials is indeed not homogenous, hence some different phases can coexist, maybe in a larger length scale, as the different kinds of charge-ordered stripes.

For these three kinds of charge-ordered stripes, we simulated the charge-ordered stripes both along the a and c directions (Fig. 2). The a-direction stripe and the c-direction stripe of the same kind have similar lattice energy (the maximum difference is 0.06 eV) and similar lattice parameters. Hence, we propose that charge ordering not only takes place along the a direction but also along the c direction. Our results support the results given by Chen *et al.*[4] and Ferández-Díaz *et al.*,[6] but are different from what was suggested by Radaelli *et al.*[7] and Wang *et al.*[8]

We also noticed the proposed orbital direction of Mn^{3+} ions in the Wigner- or bistripe model.[4–8] In Fig. 2, we denote the direction with the largest Mn^{3+}-O bond length as the "orbital" of Mn^{3+} ions. Our Wigner-crystal model is exactly identical to that used by Radaelli *et al.*,[7] and our bistripe model is exactly identical to that used by Mori *et al.*[5] This is because the bond length is closely associated with the d_{z^2} orbital direction[4] of Mn^{3+} ions. It is also found that Mn^{3+} stripes have "orbitals" orientated perpendicularly to each other, just as pointed out by Mori *et al.*[5]

B. Local structure

Except for the change in lattice parameters, $La_{1/3}Ca_{2/3}MnO_3$ inherits most of the structural characteristics of $LaMnO_3$, and is closer to the ideal cubic perovskite (see Table III). We compared the Mn-O bond lengths of our Wigner-crystal configurations with the experimental results given by Radaelli *et al.*[7] Using the Winger-crystal model of $La_{0.333}Ca_{0.667}MnO_3$ (at 1.5 K), Radaelli *et al.* reported the Mn^{3+}-O bond lengths: 2.204 Å, 1.916 Å, and 1.902 Å (average value was 2.007 Å), and the six Mn^{4+}-O bond lengths were 1.94 Å with a variation less than 0.07 Å. Our calculated average Mn^{3+}-O bond lengths of the Wigner model are 2.130 Å, 1.950 Å, and 1.917 Å (average value is 2.006 Å), and the six Mn^{4+}-O bond lengths are 1.911 Å with a variation of less than 0.016 Å. The difference between the calculated and experimental bond lengths is less than 3.5%. We also compared the average Mn-O1 and Mn-O2 bond lengths of our Wigner-crystal configurations with the experimental results (at 200 K) refined from neutron data with a Wigner-crystal model in Ref. 6. The experimental Mn-O1 and Mn-O2 bond lengths were 1.9069 Å and 1.936 Å, respectively, while our calculated Mn-O1 and Mn-O2 bond lengths are 1.913 Å and 1.954 Å, respectively. The difference between calculated and observed bond lengths is less than 1.0%. These differences may be partially attributed to a small difference in lattice parameters (about 1.0%) between the calculated and observed $La_{1/3}Ca_{2/3}MnO_3$ structure [Table III(e) and III(h)–III(l)]. These small differences indicate that our simulated structure of the Winger-model can well reproduce the experimental structure.

We investigated the local structure of $La_{1/3}Ca_{2/3}MnO_3$ in detail by calculating the bond lengths of the layer-stripe configuration along the *c* direction. Figures 3(a) and 3(b) show the *c*- and *b*-axis projections of our extended supercell of the layer-stripe configuration, respectively. In Fig. 3(b), there are two La^{3+} and four Ca^{2+} along the dashed zigzag line in La/Ca-O1 plane. The eight La/Ca-Mn bond lengths of every La/Ca ion are shown in Fig. 4(a). It is found that the average La-Mn bond length is larger than the average La/Ca-Mn bond length and is very close to the average La-Mn bond length in $LaMnO_3$. But the average Ca-Mn bond length is smaller than the average La/Ca-Mn bond length and is very close to the Ca-Mn bond length in $CaMnO_3$.

In Fig. 3(b), there are two Mn^{3+} and four Mn^{4+} along the solid zigzag line in Mn-O2 plane. The six Mn-O bond lengths of each Mn ion are shown in Fig. 4(b) (bottom). It is found that the average Mn^{3+}-O bond length is larger than the average Mn^{3+}/Mn^{4+}-O bond length and is very close to the average Mn^{3+}-O bond in $LaMnO_3$. But the average Mn^{4+}-O bond length is smaller than the average Mn^{3+}/Mn^{4+}-O bond length and is very close to the Mn^{4+}-O bond in $CaMnO_3$. Figure 4(b) (top) shows the Jahn-Teller distortion (see Ref. 36 for the calculation method) of every Mn ion. The Jahn-Teller distortion around Mn^{3+} ions is smaller than that in $LaMnO_3$, whereas the distortion around Mn^{4+} ions is almost zero. Our calculation confirms that the lattice distortions are concentrated on the Jahn-Teller distorted $Mn^{3+}O_6$ octahedra and almost no distortion occurs on the $Mn^{4+}O_6$ octahedra,[4] and it confirms also that the Jahn-Teller distortions along Mn^{3+} stripes are in fact Jahn-Teller "sheets."[5]

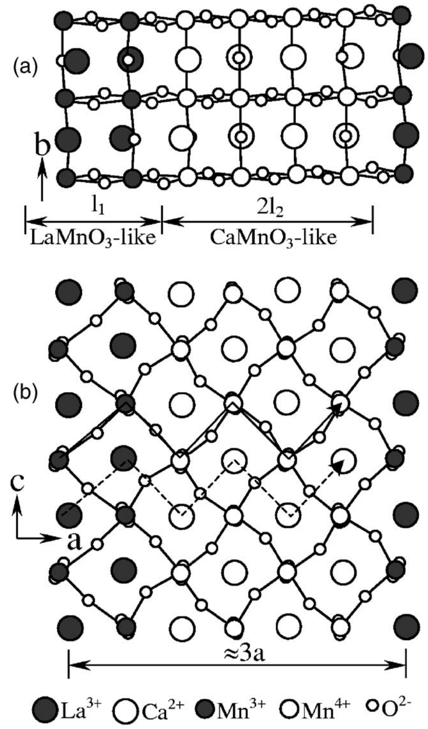

FIG. 3. The c-axis projection (a) and b-axis projection (b) of the layer-stripe model of $La_{1/3}Ca_{2/3}MnO_3$. The covered atoms are not shown.

According to the calculated bond lengths, the supercell shown in Fig. 3 can be divided as two parts: $LaMnO_3$-like layer with width of l_1 which contains La^{3+} and Mn^{3+} ions, and $CaMnO_3$-like layer with width of $2l_2$ which contains Ca^{2+} and Mn^{4+} ions. Moreover, if we consider the layered stripe as a lattice cell: the lattice space of $LaMnO_3$-like stripe is $l_1 = 5.825$ Å, while the lattice space of $CaMnO_3$-like stripe $l_2 = 5.167$ Å. l_1 is larger than l_2 by about 13%, namely, expansion takes place in $LaMnO_3$-like stripe, and contraction in $CaMnO_3$-like stripe. From high-resolution electronic microcopy (HREM) images of $La_{1/2}Ca_{1/2}MnO_3$, Mori *et al.*[5] found lattice contraction in paired stripes and dilation in nonpaired stripes. Combining the bond lengths and the contraction and expansion in the layered stripes, we believe that the local structure of $La_{1/3}Ca_{2/3}MnO_3$ is very different from the average structure.

Some experimental results showed that the local structure of doped manganites is not homogenous. It was reported that the change in the MnO_6 octahedra in $La_{0.7}Ca_{0.3}Mn_{1-x}Sc_xO_3$ ($x = 0$ to 0.3) partially caused the strong dependence of T_C on x.[37] Upon doping, the bond-length splitting in $La_{1-x}Sr_xMnO$ was significantly reduced when x increased from 0 to 0.3, and this reduction may be attributed to the partial charge

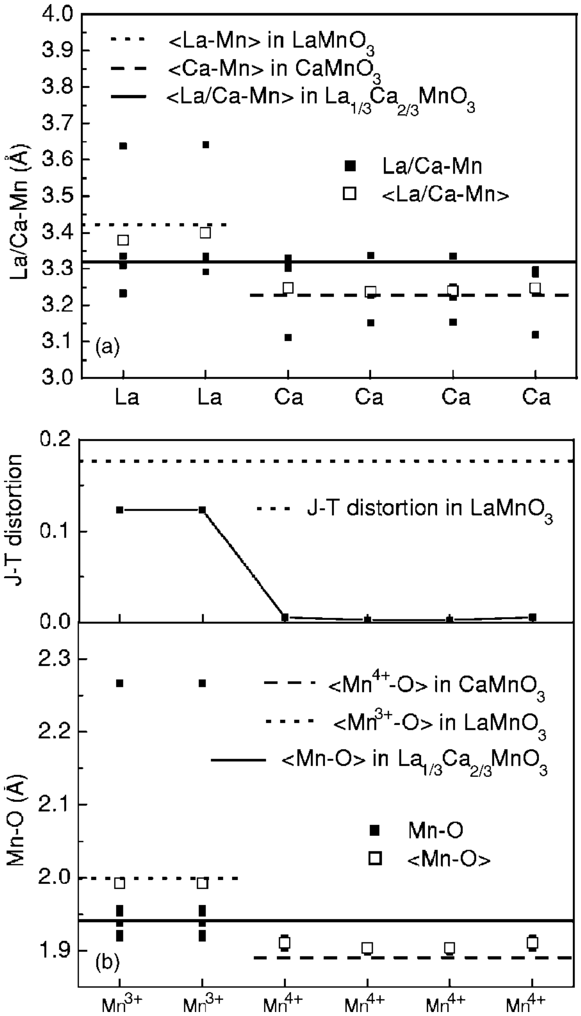

FIG. 4. Local structure of the layer-stripe model in Fig. 3: La/Ca-Mn bond length (a), Mn-O bond length [bottom of (b)], and Jahn-Teller distortion [top of (b)]. The notation ⟨ ⟩ denotes average value.

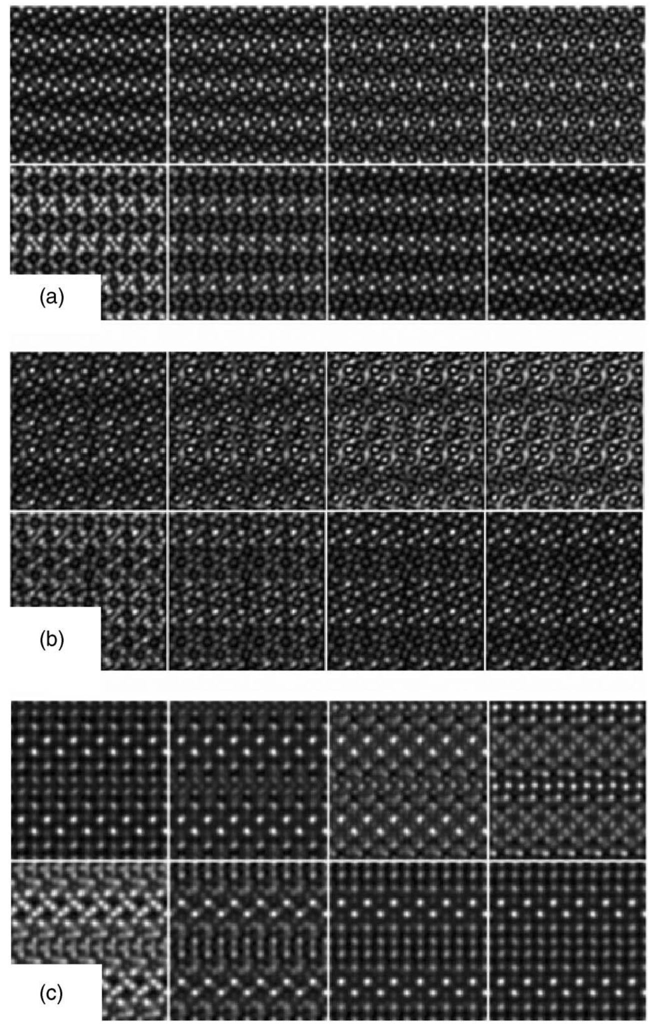

FIG. 5. Calculated HREM images for a Wigner stripe (a), a bistripe (b), and a layer stripe (c). The energy of incident electron beam is 200 keV without crystal tilt. Crystal thickness for simulation for (a) and (b) is 24 nm and for (c) is 27 nm. From left to right and from top to bottom, the defocuses are −40, −45, −50, −55, −60, −65, −70, −75 nm for (b) and (c), and −20, −25, −30, −35, −40, −45, −50, −55 nm for (a).

transfer between the Mn ions by the double exchange mechanism.[11] In $La_{1/2}Ca_{1/2}MnO_3$, examination of the local structure from Mn-O and Mn-Mn correlations revealed three distinct regions in the structure-field diagram.[38] Our simulation results show similar structural features as these experimental findings.

From another point of view, the existence of the $LaMnO_3$-like and $CaMnO_3$-like local structure in $La_{1/3}Ca_{2/3}MnO_3$ indicates a local chemical inhomogeneity. The chemical inhomogeneity in doped manganites has been confirmed by some experiments. A tendency for Sr clustering was observed in lightly doped $La_{1-x}Sr_xMnO_3$.[11] The local structure disorder in the vicinity of the clustered Sr ions was significantly smaller than that in the vicinity of La ions, presumably attributed to a higher average Mn^{3+} concentration near the La regions. La-site ordered films of $La_{2/3}Ca_{1/3}MnO_3$ prepared via atomic layer-by-layer epitaxy consisted of two layers of $LaMnO_3$ and one layer $CaMnO_3$.[17] In $La_{0.7}Ca_{0.3}MnO_3$, two spatially separated regions ($\leqslant 30$ Å) have been found, and this spatial inhomogenity was suspect to be related to the distribution of La and Ca ions and the corresponding fluctuation in the local lattice distortions.[39] This presumption and suspection are consistent with our $LaMnO_3$-like stripes in our charge-ordering models. We believe that such chemical inhomogeneity along with the different local strucutre will be crucial to theoretical study of these compounds, particularly in the context of magnetoelectronic phase separation. In contrast, some experiments found chemical homgeneity in these compounds. We believe that this discrepancy may be caused by the different probe area of the experiments (x-ray diffraction or ED). The electron beam microanalysis with ~30 nm probe did not detect any chemical imhomogeneity of La or Ca ions in phase separation or charge ordering.[40] As the chemical inhomogeneity occurs only in a small area of about one to a few nanometers as our results revealed, the electron beam microanalysis with a small probing area is needed.

In order to investigate further the atomic distribution and local structure, we calculated some HREM images (Fig. 5) based on the supercells generated by extending our simulation supercells twice along both the *a*- and *c*-axis directions. For the Wigner-crystal model, the white atomic stripes have the same spacing $a_{CO}/2 \approx 8.25$ Å as the dark atomic stripes [Fig. 5(a)]. This result is similar to some experimental and calculated HREM images given by Wang *et al.*,[8] who have observed a superlattice with a fringe period of $a_{CO}/2 = 8.1$ Å. Our HREM images of the bistripe or layer-stripe model [Fig. 5(b) and 5(c)] also show different densities of stripes with different widths. We found that the contrast of the simulated HREM images is very sensitive to the thickness and the selected parameters. Agreeing with the suggestion given by Wang *et al.*,[8] we also suggest that charge ordering can introduce contrast in HREM images by different local chemistry composition, especially by different local structure.

IV. CONCLUSION

Using atomistic simulation, we studied the possible charge-ordered stripes and local structure in $La_{1/3}Ca_{2/3}MnO_3$. It is found that La/Ca ordering along with Mn^{3+} and Mn^{4+} stripes is more energetically favorable than La/Ca disordering at low temperatures (0–50 K). It is also found that besides the Wigner-stripe model and the bistripe model, there exists a new possibly charge-ordered model: the layer-stripe model. These three kinds of charge-order stripes are more energetically preferable than random configurations, and these stripes can be formed along both the *a*- and *c*-directions. The local structure in the layer-stripe model is found to be quite different from the average structure: $LaMnO_3$-like and $CaMnO_3$-like local structures are formed. Such cation distribution and the different local structure may be a compositional representation of phase separation in doped manganites.

ACKNOWLEDGMENTS

The authors would like to thank the Ministry of Science and Technology of China (Grants No. TG2000067108 and No. 2002CB613500) and National Science Foundation of China (Grant No. 90401013) for financial support. One of the authors (F.L.T.) would also like to thank Chen Jun for her help in HREM image calculation.

*Corresponding author. Electronic address: xzzhang@tsinghua.edu.cn

[1] E. Dagotto, T. Hotta, and A. Moreo, Phys. Rep. **344**, 1 (2001).
[2] M. B. Salamon and M. Jaime, Rev. Mod. Phys. **73**, 583 (2001).
[3] A.-M. Haghiri-Gosnet and J.-P. Renard, J. Phys. D **36**, R127 (2003).
[4] C. H. Chen, S.-W. Cheong, and H. Y. Hwang, J. Appl. Phys. **81**, 4326 (1997).
[5] S. Mori, C. H. Chen, and S.-W. Cheong, Nature (London) **392**, 473 (1998).
[6] M. T. Fernández-Díaz, J. L. Martínez, J. M. Alonso, and E. Herrero, Phys. Rev. B **59**, 1277 (1999).
[7] P. G. Radaelli, D. E. Cox, L. Capogna, S.-W. Cheong, and M. Marezio, Phys. Rev. B **59**, 14440 (1999).
[8] R. Wang, J. Gui, Y. Zhu, and A. R. Moodenbaugh, Phys. Rev. B **61**, 11946 (2000).
[9] C. de Graaf, C. Sousa, and R. Broer, Phys. Rev. B **70**, 235104 (2004).
[10] R. Mathieu, D. Akahoshi, A. Asamitsu, Y. Tomioka, and Y. Tokura, Phys. Rev. Lett. **93**, 227202 (2004).
[11] T. Shibata, B. Bunker, J. F. Mitchell, and P. Schiffer, Phys. Rev. Lett. **88**, 207205 (2002).
[12] Y. Ueda and T. Nakajima, J. Phys.: Condens. Matter **16**, S573 (2004).
[13] F. Millange, V. Caignaert, B. Domengès, B. Raveau, and E. Suard, Chem. Mater. **10**, 1974 (1998).
[14] O. Chmaissem, B. Dabrowski, S. Kolesnik, J. Mais, J. D. Jorgensen, S. Short, C. E. Botez, and P. W. Stephens, Phys. Rev. B **72**, 104426 (2005).
[15] D. Akahoshi, M. Uchida, Y. Tomioka, T. Arima, Y. Matsui, and Y. Tokura, Phys. Rev. Lett. **90**, 177203 (2003).
[16] G. Banach and W. M. Temmerman, Phys. Rev. B **69**, 054427 (2004).
[17] A. Palanisami, M. Warusawithana, J. N. Eckstein, M. B. Weissman, and N. D. Mathur, Phys. Rev. B **72**, 024454 (2005).
[18] C. R. A. Catlow and G. D. Price, Nature (London) **347**, 243 (1990).
[19] C. R. A. Catlow, R. James, W. C. Mackrodt, and R. F. Stewart, Phys. Rev. B **25**, 1006 (1982).
[20] D. J. Harris, G. W. Watson, and S. C. Parker, Phys. Rev. B **56**, 11477 (1997).
[21] H. Donnerberg, S. M. Tomlinson, C. R. A. Catlow, and O. F. Schirmer, Phys. Rev. B **44**, 4877 (1991).
[22] E. Bourova, S. C. Parker, and P. Richet, Phys. Rev. B **62**, 12052 (2000).
[23] P. D. Battle, T. S. Bush, and C. R. A. Catlow, J. Am. Chem. Soc. **117**, 6292 (1995).
[24] X. Zhang and C. R. A. Catlow, Phys. Rev. B **46**, 457 (1992).
[25] X. Zhang and C. R. A. Catlow, Phys. Rev. B **47**, 5315 (1993).
[26] X. Zhang, K. W. Yip, and C. K. Ong, Phys. Rev. B **51**, 1277 (1995).
[27] X. Zhang, C. R. A. Catlow, and W. Zhou, Physica C **168**, 417 (1990).
[28] X. Zhang and L. Wang, J. Phys. Chem. Solids **64**, 1207 (2003).
[29] J. Gale and A. L. Rohl, Mol. Simul. **29**, 291 (2003).
[30] B. G. Dick and A. W. Overhauser, Phys. Rev. **112**, 90 (1958).
[31] I. Loa, P. Adler, A. Grzechnik, K. Syassen, U. Schwarz, M. Hanfland, G. K. Rozenberg, P. Gorodetsky, and M. P. Pasternak, Phys. Rev. Lett. **87**, 125501 (2001).
[32] M. Pissas and G. Kallias, Phys. Rev. B **68**, 134414 (2003).
[33] Y. X. Wang, Y. Du, R. W. Qin, B. Han, J. Du, and J. H. Lin, J. Solid State Chem. **156**, 237 (2001).
[34] J. C. Loudon and P. A. Midgley, Phys. Rev. B **71**, 220408(R) (2005).
[35] J. Tao, D. Niebieskikwiat, M. B. Salamon, and J. M. Zuo, Phys. Rev. Lett. **94**, 147206 (2005).

[36] F. L. Tang and X. Zhang, J. Phys.: Condens. Matter **17**, 6507 (2005).

[37] A. N. Ulyanov and S.-C. Yu, J. Appl. Phys. **97**, 10H702 (2005).

[38] T. A. Tyson, M. Deleon, M. Croft, V. G. Harris, C.-C. Kao, J. Kirkland, and S.-W. Cheong, Phys. Rev. B **70**, 024410 (2004).

[39] R. H. Heffner, J. E. Sonier, D. E. MacLaughlin, G. J. Nieuwenhuys, G. Ehlers, F. Mezei, S.-W. Cheong, J. S. Gardner, and H. Röder, Phys. Rev. Lett. **85**, 3285 (2000).

[40] C. H. Chen and S.-W. Cheong, Phys. Rev. Lett. **76**, 4042 (1996).